JOURNAL OF Materials CHEMISTRY

Thermal behavior and texture of mesoporous zirconia obtained from anionic surfactants

E. Zhao,[a] O. Hernández,[a] G. Pacheco,[b] S. Hardcastle[c] and J. J. Fripiat*[b]†

[a] *Department of Chemistry and Laboratory for Surface Studies and* [b] *Departmento de Ciencia de Materiales, ESFM Edif. 9, UPALM Zacatenco 07738, Mexico, DF*

[c] *Advanced Analytical Facility, University of Wisconsin-Milwaukee, P.O. Box 413, Milwaukee, WI 53201, USA*

Thermogravimetric and differential thermal analyses of mesoporous zirconias obtained from anionic surfactants by a scaffolding mechanism reveal interesting differences between the samples prepared from long-chain sulfates or sulfonates, which lose their hydration water in two steps, and those obtained from long-chain phosphates for which dehydration occurs in one step. From the temperature of the tetragonal to monoclinic transition the molar volume of ZrO_2 undergoing this transformation can be calculated. From the density and from the mesoporous volume (N_2 adsorption), the thickness of the wall separating the elemental volumes of the mesoporous structure can be calculated as well as the pseudo-length of the pores. The calculated surface area of the mesopore fits nicely with the measured *T*-plot surface area for the sample calcined at 500 °C. For the sample dried at 140 °C, the agreement is not as good, probably because of a more disordered organization. The alkyl chain is tilted by about $57 \pm 10°$ with respect to the normal to the wall. Upon calcination the thickness of the wall increases to a point where crystallization in monoclinic zirconia occurs. At this point the mesoporous character is lost.

In order to explain the processes of formation of mesoporous zirconia mediated by anionic surfactants, we have suggested a scaffolding mechanism,[1,2] which is related to that initially proposed by Hudson and Knowles[3] for a different process involving cationic surfactants. They had prepared mesoporous ZrO_2 with alkyltrimethylammonium first by precipitating a positively charged zirconium hydrogel, then by inverting the charge with ammonia followed by a cation exchange, ammonium–organic ammonium surfactant. Their procedure yields a material which develops mesoporosity only after the removal of the surfactant, as in the templating mechanism of formation of mesoporous silica and other oxides.[4–13]

The preparation of mesoporous zirconia with anionic surfactant yields solids, developing mesoporous volumes between 0.2 and 0.6 ml g^{-1} and *T*-plot areas[14] between 150 and 450 m^2 g^{-1}. Translated per ZrO_2 unit the larger values are similar to that reported for templated SiO_2.[4,11,12] In this paper, we chose to call the *T*-plot area the Lippens and de Boer method[14] for determining the mesopore area instead of the usual abbreviation '*t*-plot', in order to avoid confusion with the wall thickness, t (*vide infra*).

The organizations of the 'templated' or 'scaffolded' materials are different, as are their thermal behaviors. These differences justify the use of a different name. The porosity is not accessible in a templated material unless the surfactant is removed. In contrast, it is accessible in scaffolded materials as defined herein. A templated material is well ordered, while the scaffolded material is disordered.

We suggested that scaffolding leads to the formation of the idealized molecular architecture shown in Fig. 1, adapted from ref. 1. A positively charged ZrO_2 oligomer adsorbed the surfactant, perhaps, by hydrogen bonding, and mixed organic/inorganic sheets with a thickness (t) between 1 and 2 nm are formed and aggregate into polygonal (square is just used for convenience) prisms of length L. The small-angle XRD reflection is the repeated S distance. The pore size, approximated by $S-t$, was between 2 and 7 nm. These data were obtained through the following equations.

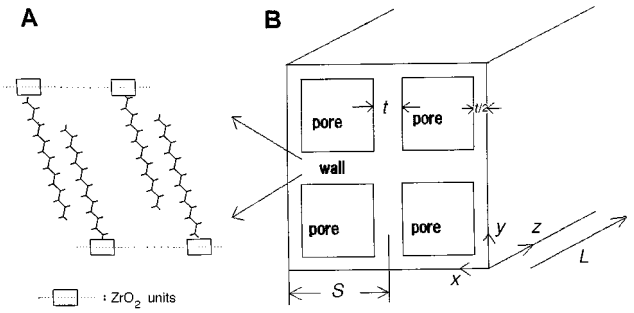

Fig. 1 Schematic model illustrating the scaffolding mechanism. (A) A wall fragment. (B) Porous structure. Adapted from ref. 1.

If the gel consists of the repetition of $n_x n_y n_z$ subunits along the x and y axes, while L is the extension along the z axis, then the volume of matter, V_m, is

$$V_m = L[(S+t)^2-(S-t)^2]n \quad (1)$$

and the void volume, V_o, is

$$V_o = L(S-t)^2 n \quad (2)$$

with $n = n_x n_y n_z$. From eqn. (1) and (2) and the definition of the density ρ arises

$$\rho V_o = (r^2-1)^{-1} \quad (3)$$

where

$$r^2 = \left(\frac{S+t}{S-t}\right)^2 = [1+(\rho V_o)^{-1}] > 1$$

and where unambiguously, in the frame of the model, the wall thickness t is

$$t = S\left(\frac{r-1}{r+1}\right) < S \quad (4)$$

The density ρ was obtained through approximations to be discussed later. The experimental support for this reasoning came from three types of experimental results.[1,2]

†E-mail: Jose@csd.uwm.edu

High resolution transmission electron microscopy carried out on two mesoporous ZrO_2 revealed, in thin regions of preparation, disordered aggregates of polygonal holes in samples dried at 140 °C. Their diameters fitted by a normalized Gaussian were in the order of 4 nm, while the calculated ones [eqns. (1)–(4)] were between 3.5 and 4.5 nm.

In spite of the generally poor quality of the pore-size distribution function obtained from the N_2 desorption isotherm and calculated using the BJH algorithm,[15] there was a crude agreement with the dimensions obtained from HRTEM and the diameter beyond which the pore-size distribution function falls to zero.

We did not explain the relatively large variations observed between different preparations made by following the same procedure. However, we did observe systematic differences between hydrolysis 'catalysts,' either H_2SO_4 (with the sulfate or sulfonate surfactant), or H_3PO_4 (with the dodecylphosphate) or HCl. When hydrolysis is performed with H_2SO_4 and alkyl sulfate or sulfonate, or with H_3PO_4 and alkyl phosphate, the pore volume of the solid dried at 140 °C is almost double that measured when HCl is used. Phosphate was introduced in the structure, according to ^{31}P NMR results,[1] and it is known that sulfate stabilizes the zirconia tetragonal structure.[13]

The fundamental aim of this contribution is to provide additional arguments in favor of the scaffolding mechanism in the framework of the study of mesoporous zirconia. For the sample dried at 140 °C for which the surfactant load is known, the density of the organic part was assumed to be unity, whereas that of the Zr oligomer was taken as equal to 3.2 g cm^{-3}.[16] After calcination, the density was assumed to be that of tetragonal zirconia, *ca.* 5.6 g cm^{-3}.[16]

In the present work the phase changes resulting from thermal treatment are examined in recording powder X-ray diffractograms at increasing temperatures, and by carrying out differential thermal analyses (DTA) and thermogravimetric analyses (TGA). It will be shown that by using density values founded on physical determination, it is possible to calculate the internal pore area and compare it with that obtained from the *T*-plot, which is applicable to mesoporous solids. Since the *T*-plot area is not used in eqn. (1)–(4), this prediction supports the model and any agreement would be independent.

In the meantime, the influence of the hydrolysis pH and of the hydrolysis catalysts will become clearer.

Experimental

Reagents and preparation procedure

The reagents and preparation procedure were those used in ref. 1, so they will only be briefly summarized here.

The following surfactants were used in this work: (a) Fisher: sodium lauryl sulfate, ($S_{529\text{-}500}$, Lot 961958), CH_3–$(CH_2)_{10}$–CH_2OSO_3Na, abbreviated as Sf_{12}. The Sf_{12} aqueous solution contained 3.5×10^{-3} mol surfactant per 30 ml; (b) Acros: sodium 1-hexadecyl sulfonate (41139-0250, Lot A13000), CH_3–$(CH_2)_{14}$–CH_2OSO_2Na, abbreviated as So_{16}. The So_{16} aqueous solution contained 3.1×10^{-3} mol surfactant per 30 ml; (c) monododecyl phosphate, $(C_{12}H_{25}O)PO(OH)_2$, abbreviated as P_{12}. The P_{12} aqueous solution contained 3.8×10^{-3} mol surfactant per 30 ml. The source of zirconium was a 70 wt% solution of zirconium propoxide in propan-1-ol (Aldrich: 33,397-2, Lot 05301 KQ), abbreviated as Zr-prop.

The synthesis was carried out in three steps. First, 10 ml of the Zr-prop solution was placed in a glass reactor at 0 °C and using an automatic burette, the surfactant solution was added at a rate of 6 ml h^{-1} with stirring. A dry N_2 flow of 50 ml min^{-1} prevented the spontaneous hydrolysis of Zr-prop, upon contact with moisture. The pH of the surfactant/water–propanol solution was adjusted initially to values close to 2, using either HCl, H_2SO_4 or H_3PO_4. The hydrolysis step was followed immediately by an aging step where the suspension of hydrolyzed zirconia in the surfactant solution was stirred for 12 h at 40 °C. The final pH was then measured. At the end of the first aging step, the solid was removed from the reactor and transferred into a hydrothermal stainless steel pressure tube containing between 5 and 10 ml of water, and heated at 140 °C for 48 h with continuous end-over-end rotation. After cooling, the solid was removed from the tube and transferred into a centrifuge tube with about 20 ml water and washed once more by centrifugation. Then, it was dried at 140 °C for 2 h. A part of it was calcined in air at 500 °C for 12 h, at a heating rate of 250 °C h^{-1}.

Physical characterization

(a) PXRD. High-angle PXRD between 10 and 75° 2θ was obtained with a Scintag θ–θ X-ray diffractometer (Cu-Kα) with the following set of slits: 3, 2, 0.5 and 0.3 °C. The scanning rate was 5° min^{-1} and a solid state detector was used. Samples were heated for 12 h at increasing temperatures between 500 and 1000 °C. The low-angle PXRD results can be found in ref. 1 where they were discussed at length.

(b) Adsorption isotherms. N_2 adsorption and desorption isotherms were obtained with an automated physisorption instrument operated in static mode (Omnisorp 100, Coulter Co.). All measurements were performed after outgassing the sample at 150 °C under vacuum, down to a residual pressure better than 10^{-4} Torr.

(c) DTA–TGA. The thermograms were obtained with a Setaram instrument at a heating rate of 10 °C min^{-1}.

Results

The physical and chemical characterizations were performed on the solids dried at 140 °C or calcined at 500 °C, or higher temperatures up to 1000 °C. The samples are designated according to the surfactant used (*e.g.* Sf_{12}), the particularities of the procedure [*e.g.* Sf_{12} (5)], and the final thermal treatment [*e.g.* Sf_{12} (5) 140 °C]. Table 1 summarizes the preparation conditions and the porosity characterization of the studied samples. Most of these data are taken from ref. 1. Typical examples of DTA–TGA traces are shown in Fig. 2.

While the weight loss is continuous for the P_{12} samples, a plateau extending from 300–600 °C is consistently observed for the Sf_{12} and So_{16} samples. On the DTA curve an endotherm occurs below 100 °C, probably caused by the rehydration

Table 1 Preparation conditions and porosity characteristics of the samples (see ref. 1)

			140 °C solids		500 °C solids	
sample	pH init.-fin.	acid used	V_o/ml g^{-1} [e] $1.5\leqslant\phi\leqslant10$	*T*-plot/ m^2 g^{-1}	V_o/ml g^{-1} [e] $1.5\leqslant\phi\leqslant10$	*T*-plot/ m^2 g^{-1}
Sf_{12} (5)	2–6	HCl	0.266	220	0.092	78
Sf_{12} (8)	2–7.5	H_2SO_4	0.404	335	0.125	116
So_{16} (1)[d]	2–7.0	HCl	0.120	93	0.130	95
So_{16} (2)	2–7.0[a]	HCl	0.288	247	0.131	115
So_{16} (3)	2–7.3[b]	H_2SO_4	0.562	452	0.140	120
P_{12} (1)[d]	1–3.0	HCl	0.375	291	0.254	200
P_{12} (2)	1–3.0	HCl	0.188	155	0.110	87
P_{12} (4)	2–3.8	H_3PO_4	0.433	355	0.263	227
P_{12} (5)	2–4.7[c]	HCl	0.439	384	0.118	103
P_{12} (6)	1.8–2.7	H_3PO_4	0.611	455	0.471	380
P_{12} (9)	1.8–3.0	H_3PO_4	0.609	450	0.53	398

Volume propanol/volume (propanol + water): [a]43%; [b]30% and [c]30%. All others: 10%, corresponding to the propanol content of the Zr-prop, propanolic. [d]In these preparations the zirconium propoxide was added to the surfactant solution. [e]Diameter between 1.5 and 10 nm.

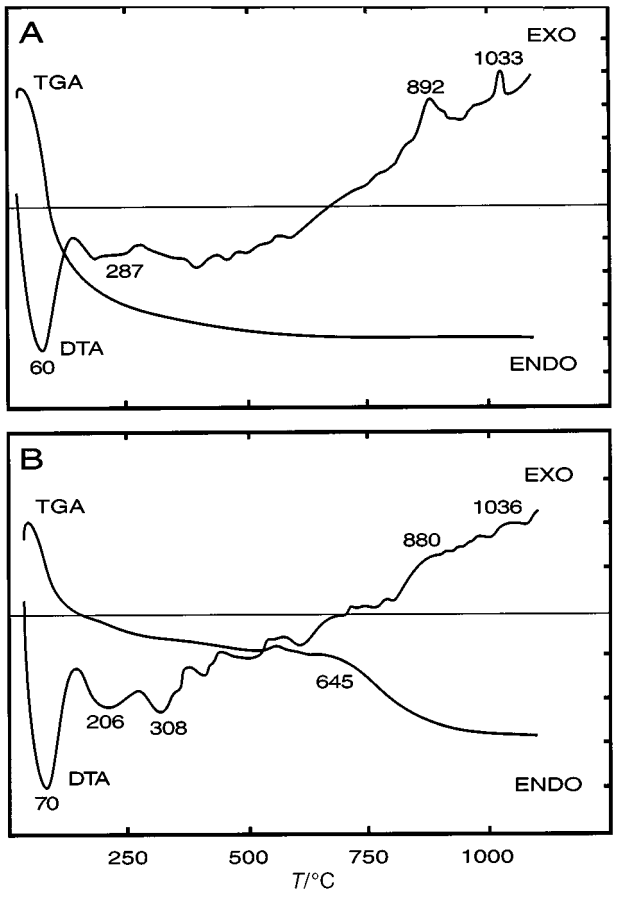

Fig. 2 Examples of thermogravimetric and differential thermal analyses obtained with sample P_{12} (4), A and sample Sf_{12} (5), B. Heating rate: 10 °C min^{-1}.

water, readsorbed by the samples either dried at 140 °C or calcined at 500 °C. Between 200 and 500 °C the DTA curve contains several ill-defined endotherms. It is in this region that the pyrolysis of the surfactant occurs, since no carbon is detectable after calcination (in air) at 500 °C.

At higher temperatures one and sometimes two exothermic peaks are observed, the first being generally less well defined than the second. These data are summarized in Table 2, where the phase changes observed by PXRD are summarized. Fig. 3 shows in more detail the evolution of the XRD pattern observed for Sf_{12} (8), So_{16} (3) and P_{12} (6). They are representative of those obtained for the other samples of the same family. It has been shown earlier[1] that the acid hydrolysis product of zirconium propoxide calcined at 500 °C was monoclinic and the particle size increased dramatically as crystallization occurred.

The mesoporous zirconia obtained with the alkyl sulfate or sulfonate remains tetragonal up to about 800 °C. As already outlined by others, sulfate inhibits the transformation tetragonal→monoclinic.[7] Similarly, phosphate prevents crystallization into the tetragonal phase. This is evident in comparing the mesoporous volumes, V_o, of the 140 °C or of the 500 °C samples, when the hydrolysis is catalyzed by HCl, H_2SO_4 or H_3PO_4 (Tables 1 and 2).

In all cases, the low-angle XRD line is observed for all samples calcined up to the temperature when crystallization into the monoclinic phase occurs.

Table 2 contains two types of information which are important for the purpose of this paper. The first concerns density, ρ [eqn. (3)]; for the 500 °C sample the density was either that of tetragonal zirconia, namely 5.6 g cm^{-3} (ref. 16) or that of amorphous zirconia, *i.e.* 3.2 g cm^{-3} (ref. 16). In ref. 1 the density was taken as 5.6 for all samples: it was not realized that the P_{12} samples are either poorly crystallized or amorphous after heating at 500 °C. The density of the samples dried at 140 °C was estimated as the weighed average of the organic part (*ca.* 1) and that of the Zr oligomer [Table 2, ρ(140 °C)].

According to the model in Fig. 1, the role of the surfactant is to organize the ZrO_2. During calcination the surfactant burns and the oligomeric species undergo further condensation, and eventually crystallize. Above *ca.* 700 °C, the sulfate is removed;[13] the phosphate remaining at *ca.* 900 °C aggregates as $Zr_2O(PO_4)_2$, Fig. 3a.

Fig. 4 illustrates most of the experimental results in Table 1. In Fig. 4b the variable chosen to represent evolution is the chemical composition represented by the ratio surfactant/Zr, mol% (s/Zr). Two trends are apparent, namely (i) an increase in the C content in the sample dried at 140 °C as the pH increases; and (ii) a continuous loss of mesoporous volume as the s/Zr ratio increases.

In addition to increasing the positive charge of the oligomer, low pH also restricts the dissociation of the polar head, sulfate, sulfonate and phosphate, and favors a hydrogen bond link over an electrostatic bond between the oligomer and the surfactant. Such a bond may be directional.

When the solid is constructed using less surfactant, at low pH, the reorganization of the oligomer resulting from the surfactant pyrolysis is much less dramatic than that occurring for higher initial surfactant content, or for higher pH (Fig. 4a).

The change in the porosity with respect to the calcination temperature is illustrated in Fig. 5 for sample P_{12} (6) *cf.* Fig. 3a showing the structural variation). Up to 800 °C the porous volume decreases progressively, but it collapses at 900 °C as crystallization occurs. Up to 800 °C, the pore-size distribution (Fig. 5b) does not change much, except for a broadening of the distribution.

Table 2 Crystal phases after 12 h treatment at 500 and 900 °C, exotherm temperatures and densities at 500 °C, from crystal phase, [ρ(140 °C) is calculated, see text and ref. 1. Tetra: tetragonal; mono: monoclinic; Am: amorphous. Minority phases in parentheses.]

sample	cryst. phase at 500 °C	cryst. phase at 900 °C	exo 1 (C)	exo 2 (C)	ρ(500 °C)	ρ(140 °C)
Sf_{12} (5)	tetra	mono	880	1036	5.6	1.9
Sf_{12} (8)	tetra	mono(tetra)	900	—[c]	5.6	2.04
So_{16} (1)	tetra	mono	—	—	5.6	1.85
So_{16} (2)	tetra	mono	855	—[c]	5.6	2.07
So_{16} (3)	tetra	mono(tetra)[a]	—	—	5.6	2.35
P_{12} (1)	am + tetra	tetra	—	—	3.2	2.29
P_{12} (2)	tetra	tetra	—[c]	—[c]	5.6	2.38
P_{12} (4)	am	tetra (ZrP)[b]	892	1033	3.2	2.11
P_{12} (5)	tetra	tetra	728	1054	5.6	2.47
P_{12} (6)	am	ZrP + mono	918	994	3.2	2.47
P_{12} (9)	am	ZrP + mono	959	—	3.2	2.47

[a]See detailed evolution in Fig. 3c. [b]At 980 °C cubic + $ZrO(PO_4)_2$ (abbreviated as ZrP) + unknown phase. [c]No exotherm observable.

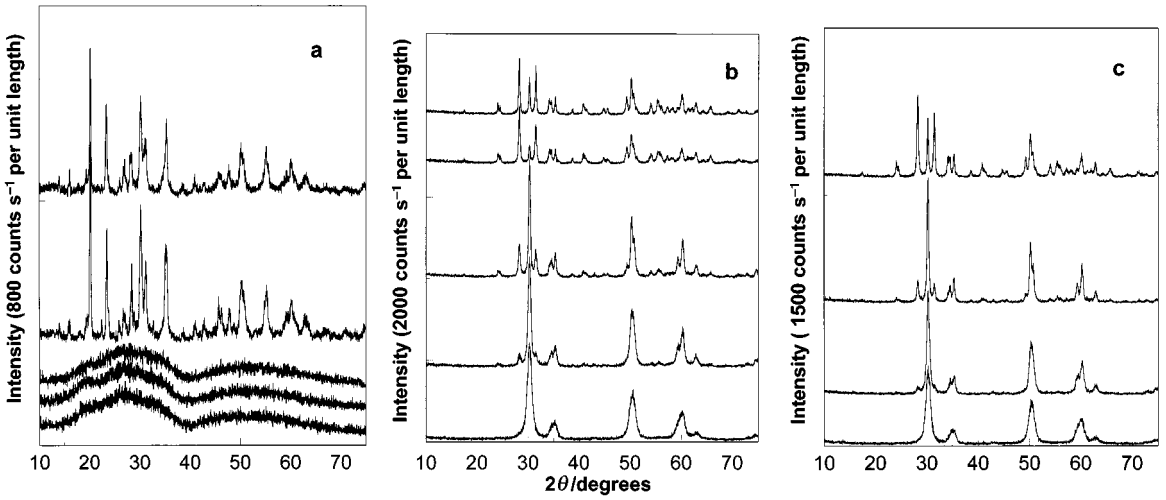

Fig. 3 Examples of PXRD patterns in the region 2θ, 10–70°. a: P_{12} (6), b: So_{16} (3) and c: Sf_{12} (8) heated at, from bottom to top 600, 700, 800, 900 and 980 °C (in a and b).

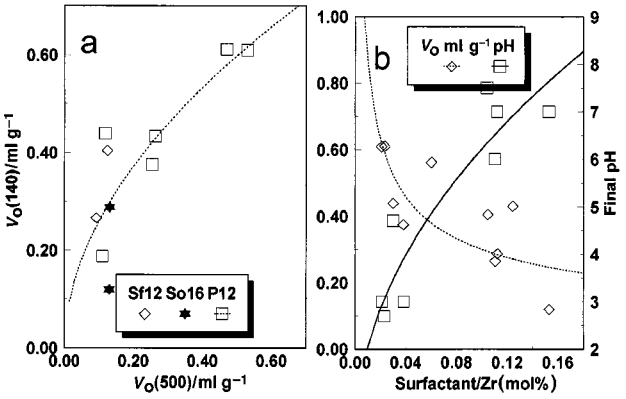

Fig. 4 a, Shrinkage of the mesoporous volume upon calcination. b, Variation of the mesoporous volume and of the 'final' pH with respect to the surfactant/ZrO_2 mol% ratio. The power regression lines show the trends.

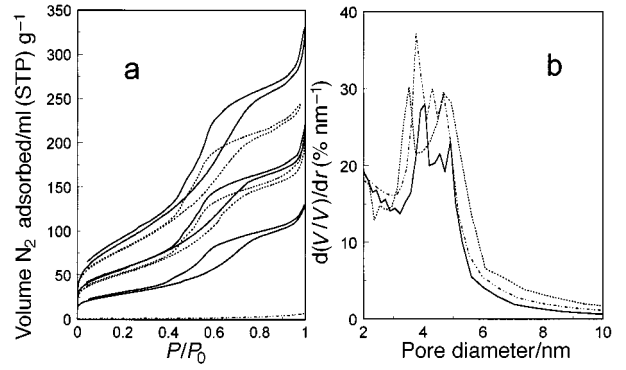

Fig. 5 N_2 adsorption isotherms (a) and pore-size distribution (b) obtained for P_{12} (6) calcined (from top) at 140, 500, 600, 700, 800 and 900 °C for 12 h. The hysteresis loop does not close for the top isotherm because of the probable existence of some microporosity. For the sake of clarity only the BJH pore-size distributions obtained at 500 (—), 600 (----) and 800 °C (···) are shown.

A similar series of experiments has also been carried out for S_{16} (3). The large change in porosity (Table 1 and Fig. 4a) occurs between 140 and 800 °C, the temperature at which the tetragonal structure is achieved. After calcination at 700 °C a further, but smaller, reduction of porous volume is obtained. At 800 °C the porous volume becomes negligible; an important fraction of the solid is monoclinic (Fig. 3b) while at 700 °C the cubic phase is present.

Discussion

As outlined above, the scaffolding of the ZrO_2 oligomers by the surfactant seems to yield a larger mesoporous volume when the oligomer is hydrogen-bonded to the surfactant (low pH). Now, it is appropriate to compare the experimental data with the parameters obtained from the model and eqn. (1)–(4) (Table 3). From eqn. (4), t is easily calculated and nL is obtained from eqn. (2); nL is the pseudo-length of the pore. (The structure is assumed to contain a single pore of 'infinite' length nL) Using nL and t, the calculated internal area (A) is

$$A = 4(S-t)nL \quad (5)$$

and it can be compared to the T-plot area shown in Table 1. Eqn. (5) is independent of the starting eqn. (1) and (2) which are second order with respect to $S-t$. Fig. 6a shows very good agreement between calculated A and the T-plot area for the 500 °C samples. The slope is about 0.8 ($R^2=0.920$) and the intercept is *ca.* 0. The densities shown in Table 2 were used. For the solid dried at 140 °C the agreement between the calculated and experimental area is poor, in the sense that the intercept is large (Fig. 6b). Possibly, in these samples the contribution of the external surface is not negligible because of smaller particle size (thin walls) as suggested by a smaller density (Table 2). For the 140 °C samples, the average ratios (t/length of the alkyl chain) are 0.41, 0.43 and 0.58 for Sf_{12},

Table 3 Wall thickness t and pore pseudo-length nL obtained by using eqn. (1)–(4) (S is the experimental low-angle XRD reflection)

	140 °C sample			500 °C sample		
sample	S/nm	t/nm	$nL/10^{-12}$ cm	S/nm	t/nm	$nL/10^{-11}$ cm
Sf_{12} (5)	4.7	1.25	2.25	5.44	1.43	5.73
Sf_{12} (8)	3.2	0.63	6.10	6.45	1.41	4.92
So_{16} (1)	3.37	1.35	2.22	7.24	1.54	4.0
So_{16} (2)	4.65	1.12	2.31	8.25	1.75	3.10
So_{16} (3)	6.1	0.85	2.04	9.1	1.84	2.66
P_{12} (1)	4.7	0.89	2.59	8.5	1.12	5.46
P_{12} (2)	4.1	1.17	2.19	6.88	1.63	3.99
P_{12} (4)	4.6	0.84	3.06	6.9	1.33	8.49
P_{12} (5)	4.65	0.76	2.83	4.81	1.09	8.52
P_{12} (6)	8.0	1.01	2.22	6.67	0.84	13.9
P_{12} (9)	6.0	0.76	2.22	(8.0)[a]	0.92	10.6

[a] Not well characterized.

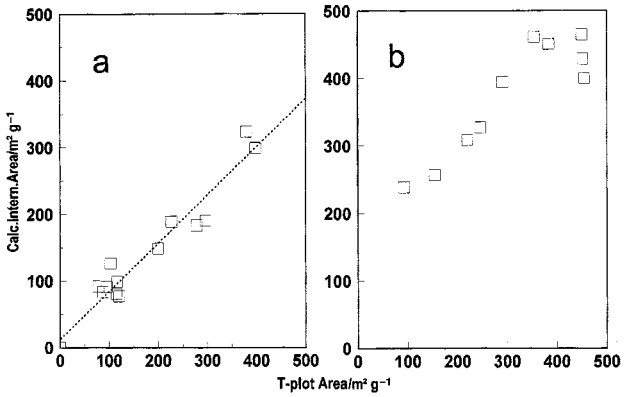

Fig. 6 Calculation of the pore internal area using eqn. (5) and the structural parameters obtained from eqn. (1)–(4) *vs.* experimental *T*-plot area. a: 500 °C solids and b: 140°C solids. The P_{12} (6) samples calcined at 600, 700 and 800 °C show similar behaviour.

So_{16} and P_{12}, respectively. These ratios suggest that the alkyl chains are tilted by an angle θ with respect to the normal to the wall: cos $\theta = t$/alkyl chain length. Average values of θ are between 45 and 65°.

The thickness of the walls in the 500 °C samples is systematically larger, suggesting a reorganization of the oligomers as they undergo further condensation. Accordingly, the pseudo-length nL decreases by almost a factor of 10, with respect to its value in the 140 °C samples. The pseudo-length is, in fact, a scaling factor. A decrease of nL can be interpreted as resulting from sintering.

More independent, experimental support for the model can be found in the thermal behavior. The increase in the wall thickness upon calcination predicted by calculation has been observed by HRTEM.[1,2]

The temperatures of the formation of the monoclinic phase, which occurs (Table 2) below 1000 °C, may also be used to approximate the size of the particle undergoing the transformation.[17–20] This tool must be used cautiously. We may consider the thickness as equivalent to the particle size and examine the relationship of the thickness to the transformation temperature. The thickness of the walls in the 500 °C sample is the one to consider, since it does not involve the surfactant. However, the thickness at the transformation temperature is not known and, as shown later, it has changed when calcination is carried out at temperatures higher than 500 °C. Nevertheless, as shown in Fig. 7a, the wall thickness is smaller for higher exo 1 temperatures. [The P_{12} (5) sample with a transition temperature of 728 °C is outside the frame.] According to the classical

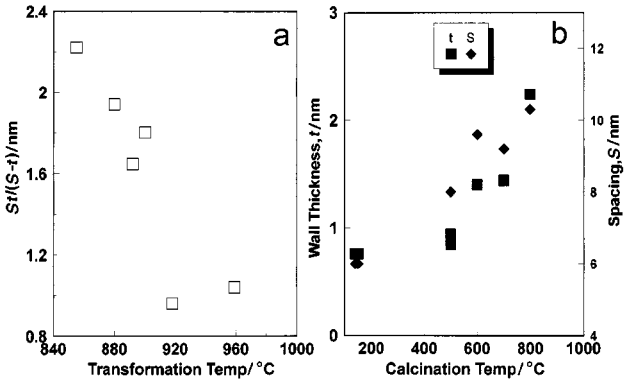

Fig. 7 a, Decrease of the $St/(S-t)$ ratio calculated for the 500 °C samples *vs.* the temperature of the first exothermic peak. Thinner walls crystallize at higher temperatures. b, Variation of the small-angle PXRD (S) and of the calculated wall thickness for sample P_{12} (6); *cf.* Fig. 4.

nucleation theory,[21] the temperature at which the phase change occurs must fit eqn. (6)

$$V_m \Delta g_b = A\Delta\gamma \quad (6)$$

where Δg_b is the bulk molar free energy and $\Delta\gamma$ is the surface free energy variation at the transition. $|\Delta g_b|$ decreases as the transition temperature increases, hence $V_m/A = St/(S-t)$ should decrease, as it does.

The structure of mesoporous zirconia is very disordered, consequently the structural parameters S and t represent averaged values of a broad distribution. It would be interesting to have some idea about their distribution functions. The width of Gaussians representing the distribution of the polygonal holes on HRTEM pictures[1] was *ca.* 1 nm. The pore-size distributions in Fig. 5b are also informative. A broadening of the distribution is observed at increasing calcination temperatures, while the maximum remains in the same range of values. The latter observation is in agreement with the results in Fig. 7b. Since both S and t increase with temperature, the difference $(S-t)$ does not vary much. Since V_o decreases noticeably as the calcination temperature increases, it must be concluded, in agreement with eqn. (2), that nL decreases. Sintering becomes active at about 800 °C, *i.e.* at the onset of the crystallization into the monoclinic and phosphate phases.

Conclusions

Mesoporous silicates, aluminosilicates and oxides are formed easily through a sol–gel process mediated by surfactants, the starting material often being an alkoxide. In most cases, the mechanism has been described as a templating process. Surfactants self-assemble in rod, disc or sphere-shaped structures onto which the alkoxide is fixed during hydrolysis. There is a direct geometrical relationship between the size of the cavity, in which the micelle is lying, and the size of the pores. Of course, no porosity available to the outside atmosphere is developed until the surfactant is removed.

When mesoporous zirconia was first obtained from zirconium propoxide using anionic surfactants, it became rapidly evident that we could not describe the synthesis process by a templating mechanism as summarized above. For instance, a large porous volume was measured before the removal of the surfactant and there was no evident geometrical relationship between the surfactant and the porous volume. Thus, a crude model was described, whereby the walls of polygonal prisms are bilayers of surfactants, molecules assembled tail-to-tail, the polar head interacting with zirconia oligomers. This formation process was called a scaffolding mechanism. In order to justify the model, one has to use indirect techniques. Low-angle PXRD repeat distances between structural units and the mesoporous volume (V_o) measured from N_2 desorption isotherms were exploited previously.[1]

In the present contribution the thermal behavior of the mesoporous zirconia gave additional information. The sulfate stabilized the tetragonal phase up to about 800 °C. Phosphate delays the crystallization up to 900 °C. With a reasonable estimate for the density and knowing the mesoporous volume, if the crude model of Fig. 1 is physically reasonable, the calculated internal area of the pore should be comparable with the experimental *T*-plot area. This check has been successful for the samples calcined at 500 °C. In addition, the calculation predicts that the crystallization temperature must be higher for thin walls,[16–19] as is observed. Finally, the diameters $S-t$ of the holes observed in the HRTEM pictures, and the pore-size diameters obtained from the N_2 desorption isotherm are within *ca.* 1–1.5 nm. For such a disordered solid this may be considered as satisfactory.

The unsatisfactory aspect is the discrepancy between the calculated area and the *T*-plot area for the solid dried at 140 °C, especially when the experimental area is lower than

$300\ m^2\ g^{-1}$. The larger disorder in the 140 °C solid may be responsible for the poorer correlation.

N.B. After submission of this paper, we were made aware of an article by Vaudry *et al.*[22] who described the preparation of pure alumina mesophases using lauric acid in ethanol/water cosolvent and aluminium *sec*-butoxide. The solids obtained in this way exhibited an XRD spacing of around 3 nm and, after calcination, at 430 °C a BET surface area up to $700\ m^2\ g^{-1}$ and pore volume in the order of $0.4\ cm^3\ g^{-1}$. The pore-size distributions showed maxima near 2 nm. These characteristics are close to those reported for the zirconias synthesized in our work.

G.P.M. wants to thank COFAA-IPN for a scholarship. The financial help of DOE grant DE-FG02-90 ER1430 is gratefully acknowledged.

References

1 G. Pacheco, E. Zhao, A. Garcia, A. Sklyarov and J. J. Fripiat, *J. Mater. Chem.*, 1998, **8**, 219.
2 G. Pacheco, E. Zhao, A. Garcia, A. Sklyarov and J. J. Fripiat, *Chem. Commun.*, 1997, 491.
3 M. J. Hudson and J. A. Knowles, *J. Chem. Soc., Chem. Commun.*, 1995, 2083; *J. Mater. Chem.*, 1996, **6**, 89.
4 J. S. Beck, J. C. Vartuli, W. J. Roth, M. E. Leonowicz, C. T. Kresge, K. D. Schmitt, C. T.-W. Chu, D. H. Olson, E. W. Sheppard, S. B. McCullen, J. B. Higgins and J. L. Schlenker, *J. Am. Chem. Soc.*, 1992, **116**, 10836.
5 Q. Huo, D. L. Margoles, U. Ciesla, D. G. Demuth, P. Feng, T. E. Gier, P. Sieger, A. Firouzi, B. F. Schmelka, F. Schüth and G. D. Stucky, *Chem. Mater.*, 1996, **6**, 1176.
6 F. Schüth, *Ber. Bunsen-Ges. Phys. Chem.*, 1995, **99**, 1306.
7 V. Ciesla, S. Schacht, G. D. Stucky, K. K. Unger and F. Schüth, *Angew. Chem., Int. Ed. Engl.*, 1996, **35**, 541.
8 J. S. Reddy and A. Sayari, *Catal. Lett.*, 1996, **38**, 219.
9 D. M. Antonelli and J. Y. Ying, *Chem. Mater.*, 1996, **8**, 874.
10 N. K. Raman, M. T. Anderson and C. F. Brinker, *Chem. Mater.*, 1996, **8**, 1682.
11 P. T. Tanev, M. Chibwe and T. J. Pinnavaia, *Nature*, 1996, **368**, 321.
12 S. A. Bagshaw, E. Prouzet and T. J. Pinnavaia, *Science*, 1995, **269**, 1242.
13 Y. Y. Huang, T. J. McCarthy and W. M. H. Sachtler, *Appl. Catal. A: General*, 1996, **148**, 135.
14 S. J. Gregg and K. S. W. Singh, *Adsorption, Surface Area and Porosity*, Academic Press, London, 982.
15 E. P. Barrett, L. G. Joyner and P. H. Halenda, *J. Am. Chem. Soc.*, 1951, **13**, 573.
16 *Handbook of Chemistry and Physics*, ed. R. C. Weast, CRC Press, Boca Raton, FL, 52nd edn., 1972, p. B156.
17 R. G. Garvie, *J. Phys. Chem.*, 1978, **82**, 219.
18 A. Chatterjee, S. K. Pradhan, A. Dakka, M. De and D. Chakravorthy, *J. Mater. Res.*, 1996, **9**, 263.
19 C. R. Aita, M. D. Wiggins, R. Whig, C. M. Scanlan and M. Gajdardziska-Josifovska, *J. Appl. Phys.*, 1996, **79**, 1176.
20 M. Gajdardziska-Josifovska and C. R. Aita, *J. Appl. Phys.*, 1994, **79**, 1315.
21 P. W. M. Jacobs and F C. Tompkins, *Classification and Theory of Solid Reactions*, in *The Chemistry of the Solid State*, ed. W. E. Garner, Butterworths Scientific Publications, London, 1955, p. 185.
22 F. Vaudry, S. Khodabandeh and M. E. Davis, *Chem. Mater.*, 1996, **8**, 1451.

Paper 8/01567H; *Received* 24*th February*, 1998